01 Mar 1983

# Homogeneous Nucleation Rate Measurements for Water Over a Wide Range of Temperature and Nucleation Rate

Ronald C. Miller

Robert J. Anderson

James L. Kassner
*Missouri University of Science and Technology*

Donald E. Hagen
*Missouri University of Science and Technology*, hagen@mst.edu



## Recommended Citation

R. C. Miller et al., "Homogeneous Nucleation Rate Measurements for Water Over a Wide Range of Temperature and Nucleation Rate," *Journal of Chemical Physics*, vol. 78, no. 6, pp. 3204-3211, American Institute of Physics (AIP), Mar 1983.
The definitive version is available at https://doi.org/10.1063/1.445236

# Homogeneous nucleation rate measurements for water over a wide range of temperature and nucleation rate

R. C. Miller,[a] R. J. Anderson,[b] J. L. Kassner, Jr., and D. E. Hagen

*Physics Department and Graduate Center for Cloud Physics Research, University of Missouri—Rolla, Rolla, Missouri 65401*

(Received 15 July 1982; accepted 31 March 1982)

An expansion cloud chamber was used to measure the homogeneous nucleation rate for water over a wide range of temperature from 230–290 K and nucleation rates of $1–10^6$ drops $cm^{-3}$ $s^{-1}$. The comprehensive and extensive nature of this data allows a much more detailed comparison between theory and experiment than has previously been possible. The expansion chamber technique employs continuous pressure measurement and an adiabatic pulse of supersaturation to give the time history of supersaturation and temperature during the nucleation. The resulting drop concentration is determined using photographic techniques. The experimental observations are presented in tabular form and from them an empirical nucleation rate formula is determined: $J = S^2 \exp[328.124 - 5.582\,43T + 0.030\,365T^2 - 5.0319E - 5T^3 - (999.814 - 4.100\,87T + 3.010\,84E - 3T^2)\ln^{-2}S]$, where $J$ is the nucleation rate in units of drops $cm^{-3}$ $s^{-1}$. $S$ is the supersaturation ratio and $T$ is the temperature in K.

## I. INTRODUCTION

Nucleation is one of the most pervasive physical phenomena known to man. It plays an important role in a wide variety of engineering processes, wherever condensation, boiling, crystallization, sublimation, and catalytic processes occur. In the biological sciences nucleation has far reaching significance in the development of bone and teeth, arteriosclerosis, arthritis, and kidney and gallstones. Studies of freezing nucleation in living cells may someday evolve an understanding of why some cells are severely damaged by freezing while others are not. Nucleation also plays an important role in geophysics. Crystalline materials are found throughout the earth's crust. In the atmosphere nucleation plays a decisive role in the evolution of precipitation in clouds. In air pollution chemistry, nucleation often figures prominently in the formation of certain aerosols. In spite of the vast role nucleation plays in environmental, biological, and industrial processes, it still remains only poorly understood.

Homogeneous nucleation from the vapor phase is the simplest form of nucleation. Nucleation enjoys a close relationship to critical point phenomena. The theory of small vapor phase clusters is directly related to the theory of viral coefficients. Moreover, the theory of the structure of clusters must in the large size limit reduce to the theory of liquids. All theories of nucleation borrow heavily on concepts evolved for homogeneous vapor phase nucleation. Therefore, this particular process plays a central role in the evolution of the whole subject.

Since the initial experiments in the latter quarter of the nineteenth century, the expansion chamber has held extremely important positions in the study of the nucleation process and in the development of particle physics. The expansion cloud chamber was initially used for qualitative measurements of condensation by such pioneers as Coulier,[1] Kiessling,[2] and Aitken,[3] Wilson[4] who performed the first meaningful quantitative measurements of condensation in dust free air, and then applied the expansion cloud chamber to the observation of the interactions of high energy charged particles.[5] A review of many cloud chamber nucleation studies was given by Mason.[6] Over the years Kassner and his associates[7,8–11] have developed the expansion cloud chamber technique to allow precision measurements of homogeneous nucleation rates of water and organic compounds.

The purpose of this paper is to present the results of an expansion cloud chamber study of the homogeneous nucleation of water over a wide range of temperature and supersaturation in a form that is readily accessible to other investigators who wish to compare various features of the theory with detailed experimental results. The expansion chamber method allows the quantitative observation of nucleation rates and not just critical supersaturations. The observed data and an empirical nucleation rate formula are presented. From the observed experimental data the reader can perform his own analysis and make comparisons with his own theoretical constructions. We believe that these data are essentially free from any influence due to droplet growth effects.[12]

## II. EXPERIMENTAL APPARATUS AND PROCEDURE

These nucleation studies were performed in a Wilson type automated expansion cloud chamber designed and constructed in this laboratory. Its basic components are shown in Fig. 1. The pool of water at the bottom provides for saturation of the sensitive volume with water vapor. Argon is used as a carrier gas. This type of cloud chamber has been described in detail by Kassner *et al.*[10] and Schmitt.[12] This same facility has already been used to study the homogeneous nucleation of ice in supercooled water.[7,13] All of the supporting sub-

[a] Presently at Central State University, Edmond, Oklahoma 73034.

[b] Presently at Morgantown Energy Research Center, Morgantown, West Virginia 26505.

 0021-9606/83/063204-08$2.10 

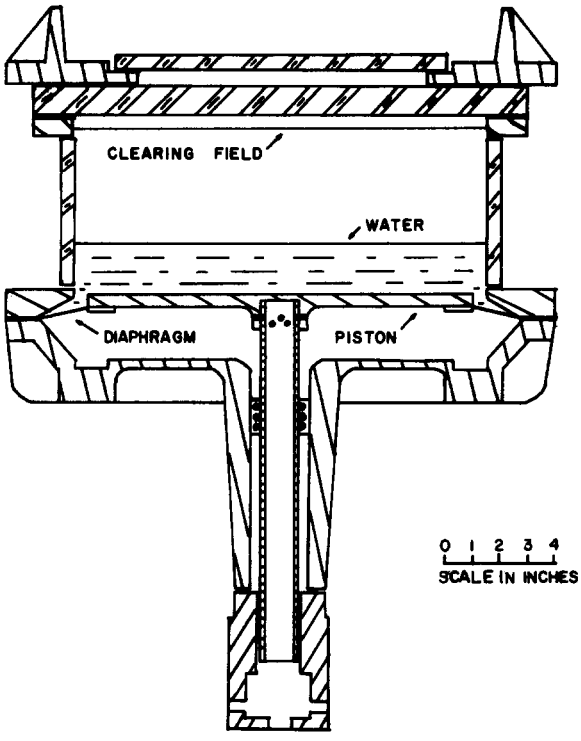


FIG. 1. The expansion chamber used for homogeneous nucleation of water studies.

systems (data acquisition and control, optics, pressure measurement, temperature measurement and control, and environmental housing) are either identical or very similar to those described by Schmitt[12] for his chamber which was used for nucleation studies of organic compounds and the reader is referred there for these details.

A number of improvements were incorporated into the present chamber. The chamber's diameter was increased to give a larger photographable area. Major improvements were made in the temperature control. A number of heater strips were attached to the chamber itself (to raise the apparatus temperature slightly above ambient), and subjected to independent control. This allowed horizontal temperature variations to be kept within 0.05 °C and a slight vertical gradient to be imposed in order to provide stability against convection. A feature was built into the controller which allowed the chamber temperature to be changed without changing the above mentioned relationships. Thus, conditions before the expansion are more easily controllable and can be changed with less effort. The expansion chamber itself is located within a well-insulated walk-in environmental chamber capable of temperatures well above and below room temperature. This provides for investigations over the wide temperature range sought here.

A vertical clearing field of ~ 70 v/cm is used to sweep ions out of the chamber's sensitive volume. Careful selection of materials and the use of both high and low supersaturation cleaning expansions kept the chamber relatively free of impurities capable of acting as heterogeneous nuclei, and allowed the homogeneous nucleation studies to extend down to low nucleation rates.[14] For normal operation only a short pulse of nucleation of the order of 0.01 s is allowed. This is achieved by a fast expansion immediately followed by a partial recompression. Figure 2 shows a typical chamber data cycle with a fast nucleation pulse. This short well-defined "sensitive time" effectively decouples the nucleation process from droplet growth effects to well within the limits of error of the experiment. Photography with subsequent drop counting is the primary method employed for drop concentration observation. The trained observer can readily distinguish certain artifacts such as cosmic ray tracks which could not be discriminated against by light scattering or transmissometry techniques. Closed

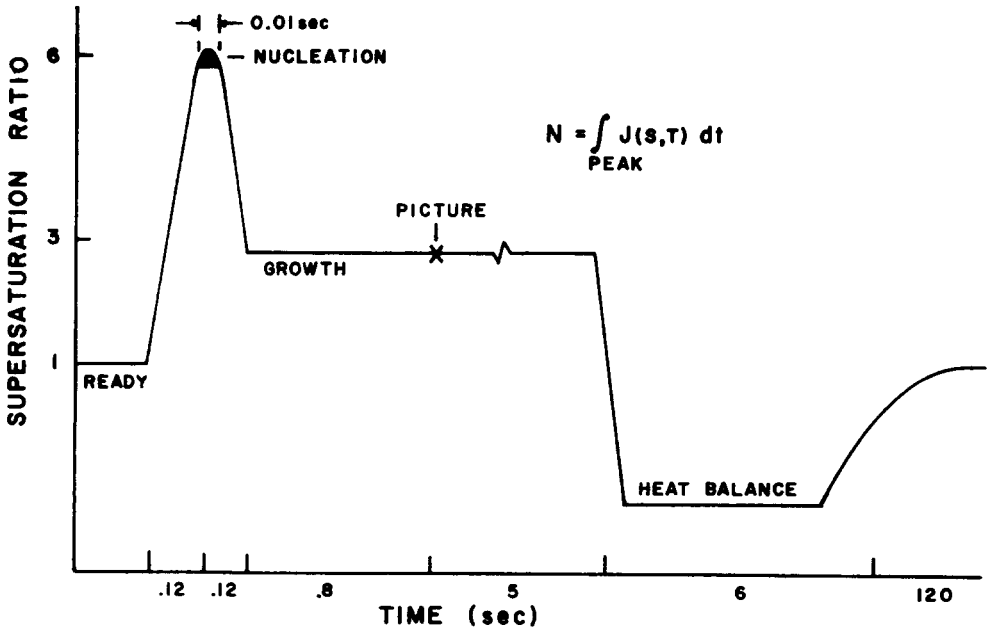


FIG. 2. Typical supersaturation ratio vs time profile.

circuit television is used in real time to check on the operating conditions of the chamber without having to enter the environmental chamber when it is operating at temperature extremes.

Cloud chamber expansions have a maximum temperature depression of ~30 °C. Therefore, to reach the lower temperatures near −43 °C sought in this investigation the cloud chamber had to have initial temperatures in the vicinity of −10 °C. Of course these low initial temperatures would freeze the distilled water ordinarily used in the base of the chamber and thus impair the operation of the chamber. For this reason a solution of NaCl and distilled water was used in the base of the chamber to prevent freezing when initial temperatures below 0 °C were employed. The freezing point of this solution is given in the Handbook of Chemistry and Physics[15] and the effect of various molalities on the vapor pressure of an aqueous saline solution is given in an article by Low.[16] The particular salt solution used for this study had a molality of 4.277 which has a freezing point of about −16.5 °C. A careful check was made to make sure that no salt nuclei were observed to evolve into the chamber sensitive volume.

To ensure that the aqueous saline solution did not affect the nucleation results, experiments without salt in the chamber water were carefully compared with experiments with salt. The same results were achieved once a small correction in the vapor pressure of the saline solution was made.

The procedure for performing the experiment consists of setting the initial temperature at some desired value via the chamber temperature controller. A period of 24 h is allowed for conditions to stabilize after the temperature setting is changed. Then a number of expansions are performed from the same initial conditions to various minimum pressures (and corresponding minimum temperatures and peak supersaturations).

Then the initial temperature setting is changed again and another set of expansions to various minimum pressures is made. The process is repeated until the desired range of temperatures is investigated. Each expansion results in a corresponding photographic record of the drop count resulting from nucleation occurring in the immediate vicinity of the peak supersaturation during the expansion.

The nucleation rate information is extracted from the above set of data; individual nucleation rates are not extracted from the results of individual expansions. The nucleation rate $J$ varies rapidly over the nucleation pulse shown in Fig. 2, reaching its maximum when the supersaturation ratio $S$ reaches its maximum. $J$ is obtained in a straightforward manner from the drop count and the time dependent conditions of supersaturation and temperature near the pressure minimum which produced the drops. The method for calculating $J$ assumes the classical functional form (suggested by Hale and Plummer[17]):

$$J = S^2 \exp[A + B/(\ln S)^2] \ . \tag{1}$$

$A$ and $B$ are of the form

$$A = x_0 + x_1 T + x_2 T^2 + x_3 T^3 \ , \tag{2}$$

$$B = x_4 + x_5 T + x_6 T^2 \ , \tag{3}$$

where $T$ is the temperature and the $x$'s are adjustable parameters, $J$ is a function of time since $S$ and $T$ are time dependent. The observed drop count (number of drops per unit volume) $N$ should equal $\int J\,dt$. A nonlinear least squares fit is done for the entire data set. Let

$$Y = \sum_{i=1}^{L} \left[ \int J(S_i(t), T_i(t))\,dt - N_i \right]^2 \ , \tag{4}$$

where $L$ is the total number of expansions, $S_i$ and $T_i$ are the time dependent supersaturation ratio and temperature profiles for the $i$th expansion, $N_i$ is the drop count for the $i$th expansion, and $J$ is given by Eq. (1). The numerical minimization routine STEPIT[18] is used to minimize $Y$ by adjusting the $x$'s in Eqs. (2) and (3).

The procedure for calculating the time dependent profiles $S_i(t)$ and $T_i(t)$ required for the evaluation of $Y$ are as follows. The pressure $P$ is directly measured with a high frequency transducer, and since the expansion is adiabatic $S$ and $T$ can be derived from $P$. The only significant nucleation and hence contribution to $\int J\,dt$ comes from the region near the pressure minimum $P_{\min}$. In this region the pressure is given by

$$P = P_{\min} + C_{P1} t + C_{P2} t^2 \ , \tag{5}$$

where $C_{P1}$ and $C_{P2}$ are coefficients that are fit to the pressure data. One set of $C_{P1}$ and $C_{P2}$ are associated with all of the expansions from one initial temperature $T_1$. "$t$" denotes the time, with $t = 0$ at the pressure minimum. In a reversible adiabatic expansion, the change in entropy is zero, or

$$dS_e = C_p (dT/T) - B_T V\,dP = 0 \ ,$$

where $S_e$ denotes the entropy, $C_p$ the heat capacity, $B_T$ the coefficient of expansion, and $V$ the gas volume. This equation refers to one mole of a single gas. For the mixture of argon and water vapor used here, the equation

$$n_a dS_a + n_w dS_w = 0$$

may be solved for $dT/T$ and numerically integrated using table values for heat capacities and coefficients of expansion to obtain the temperature $T$ as a function of pressure $P$ for given initial conditions.

With $P$ and $T$ now known the supersaturation $S$ can be calculated. It is defined as $S = p_v'/p_v(T)$, where $p_v(T)$ is the equilibrium saturation vapor pressure over a plane water surface at temperature $T$, and $p_v'$ is the adiabatic vapor pressure in the chamber

$$p_v' = p_v(T_w)(P/P_0) \ ,$$

where $P_0$ is the initial pressure and $p_v(T_w)$ is the saturation vapor pressure at the temperature ($T_w$) of the pool of water. For these experiments $T_w$ is 0.15 °C lower than the initial temperature of the sensitive experimental volume. Thus the sensitive volume, being warmer than the water due to the vertical temperature gradient needed to keep the top glass clear of condensation (for photography), is slightly undersaturated prior to the expansion.

TABLE I. Homogeneous nucleation data for selected initial temperatures. The $P$, $S$, and $T$ coefficients define the pressure, supersaturation, and temperature expansion profiles. $P_{min}$ denotes the minimum pressure, $T_{min}$ the minimum temperature, $S_{peak}$ the maximum supersaturation, $N$ the observed number density of drops homogeneously nucleated, and $\int J\,dt$ the drop density given by Eq. (8) our empirical nucleation rate. Initial temperature $T_1 = 45\,^{\circ}C$. $P$ coefficient $C_{p1} = 276.6680$, $C_{p2} = 58\,986.0$. $S$ coefficient $C_{s1} = 4.320\,94$, $C_{s2} = 20.9145$, $C_{s3} = 47.6592$, $C_{s4} = 62.0626$. $T$ coefficient $C_{t1} = 288.179$, $C_{t2} = -87.1318$, $C_{t3} = 46.1191$, $C_{t4} = -29.5823$.

| Run | $P_{min}$ | $T_{min}$ | $S_{peak}$ | $N$ | $\int J\,dt$ |
|---|---|---|---|---|---|
| 1 | 920.03 | 286.94 | 4.63 | 408.0 | 390.4 |
| 2 | 920.35 | 286.98 | 4.62 | 436.0 | 362.1 |
| 3 | 931.30 | 288.31 | 4.29 | 31.0 | 25.2 |
| 4 | 936.64 | 288.95 | 4.14 | 7.0 | 6.4 |
| 5 | 933.38 | 288.56 | 4.23 | 13.0 | 14.9 |
| 6 | 932.70 | 288.48 | 4.25 | 25.0 | 17.7 |
| 7 | 924.87 | 287.53 | 4.48 | 129.0 | 123.1 |
| 8 | 926.85 | 287.66 | 4.42 | 86.0 | 76.1 |
| 9 | 921.30 | 287.10 | 4.59 | 266.0 | 289.4 |
| 10 | 920.66 | 287.02 | 4.61 | 370.0 | 336.6 |
| 11 | 920.35 | 286.98 | 4.62 | 330.0 | 362.1 |
| 12 | 915.93 | 286.44 | 4.76 | 996.0 | 1011.5 |
| 13 | 941.47 | 286.26 | 4.81 | 1496.0 | 1411.9 |
| 14 | 915.68 | 286.41 | 4.77 | 1396.0 | 1071.2 |
| 15 | 935.55 | 288.82 | 4.17 | 6.0 | 8.5 |
| 16 | 929.24 | 288.06 | 4.35 | 46.0 | 42.2 |
| 17 | 926.17 | 287.69 | 4.44 | 96.0 | 89.8 |
| 18 | 917.84 | 286.68 | 4.70 | 616.0 | 651.0 |
| 19 | 917.53 | 286.64 | 4.71 | 716.0 | 699.5 |
| 20 | 914.75 | 286.30 | 4.80 | 1296.0 | 1324.7 |
| 21 | 933.05 | 288.52 | 4.24 | 16.0 | 16.2 |
| 22 | 931.65 | 288.35 | 4.28 | 33.0 | 23.1 |
| 23 | 923.24 | 287.33 | 4.53 | 191.0 | 182.3 |
| 24 | 919.03 | 286.82 | 4.66 | 546.0 | 493.5 |
| 25 | 913.58 | 286.16 | 4.84 | 1496.0 | 1727.7 |
| 26 | 934.12 | 288.65 | 4.21 | 17.0 | 12.3 |
| 27 | 927.20 | 287.81 | 4.41 | 56.0 | 69.8 |
| 28 | 924.19 | 287.45 | 4.50 | 126.0 | 145.1 |
| 29 | 930.61 | 288.22 | 4.31 | 30.0 | 30.0 |
| 30 | 922.27 | 287.21 | 4.56 | 196.0 | 229.8 |
| 31 | 927.54 | 287.85 | 4.40 | 76.0 | 64.2 |
| 32 | 934.84 | 288.73 | 4.19 | 10.0 | 10.3 |
| 33 | 934.12 | 288.65 | 4.21 | 12.0 | 12.3 |
| 34 | 948.89 | 290.42 | 3.82 | 0.0 | 0.2 |
| 35 | 944.08 | 289.84 | 3.94 | 0.0 | 0.9 |
| 36 | 940.58 | 289.42 | 4.03 | 0.0 | 2.3 |
| 37 | 937.34 | 289.04 | 4.12 | 3.5 | 5.4 |
| 38 | 945.32 | 289.99 | 3.91 | 0.0 | 0.6 |
| 39 | 940.55 | 289.42 | 4.03 | 0.0 | 2.3 |
| 40 | 937.71 | 289.08 | 4.11 | 1.7 | 4.9 |
| 41 | 948.49 | 290.37 | 3.83 | 0.0 | 0.3 |
| 42 | 943.70 | 289.80 | 3.95 | 0.0 | 1.0 |
| 43 | 939.54 | 289.30 | 4.06 | 0.0 | 3.0 |
| 44 | 938.10 | 289.13 | 4.10 | 2.0 | 4.4 |
| 45 | 944.54 | 289.90 | 3.93 | 0.0 | 0.8 |
| 46 | 940.28 | 289.39 | 4.04 | 0.0 | 2.5 |
| 47 | 938.09 | 289.13 | 4.10 | 1.5 | 4.4 |
| 48 | 944.54 | 289.90 | 3.93 | 0.0 | 0.8 |
| 49 | 942.21 | 289.62 | 3.99 | 0.0 | 1.5 |
| 50 | 927.01 | 289.00 | 4.13 | 3.0 | 5.9 |

The above method allows $T$ and $S$ to be evaluated as functions of pressure. It was found that these functions could be fit in the region near the pressure minimum with functions of the form

$$S(P) = C_{S1} + C_{S2}Z + C_{S3}Z^2 + C_{S4}Z^3 \,, \tag{6}$$

$$T(P) = C_{T1} + C_{T2}Z + C_{T3}Z^2 + C_{T4}Z^3 \,, \tag{7}$$

where $Z = (1200/P) - 1.29$, and the coefficients $C_{S1}$, $C_{S2}, \ldots, C_{T4}$ are fixed for each initial temperature. The units of $P$ are mmHg and $T$ is K.

## III. RESULTS

For this experiment the set of initial or pre-expansion cloud chamber temperatures 45, 35, 24.5, 13.2, 3, −3, and −9 °C were selected. The initial total pressure was fixed at 1200 mmHg. From each initial temperature a number of expansions were performed at various expansion ratios and hence various minimum pressures and temperatures at the end of the main expansion. All of the nucleation occurs in the region near the bottom of the expansion. Tables I–VII contain the results from the individual expansions, grouped according to initial temperature. The characteristics of the expansions near the bottom of the expansion are contained in the coefficients $C_{P1}$, $C_{P2}$, $C_{S1}, \ldots, C_{S4}$, $C_{T1}, \ldots, C_{T4}$ used in Eqs. (5)–(7). These coefficients are given for each initial temperature. The primary

TABLE II. See caption for Table I. Initial temperature $T_1 = 35\,^{\circ}C$. $P$ coefficient $C_{p1} = 67.0352$, $C_{p2} = 255\,949.0$. $S$ coefficient $C_{s1} = 4.\ 759\,23$, $C_{s2} = 24.4884$, $C_{s3} = 59.5091$, $C_{s3} = 91.0309$. $T$ coefficient $C_{t1} = 278.75$, $C_{t2} = -85.2922$, $C_{t3} = 45.6626$, $C_{t4} = -27.8005$.

| Run | $P_{min}$ | $T_{min}$ | $S_{peak}$ | $N$ | $\int J\,dt$ |
|---|---|---|---|---|---|
| 51 | 931.06 | 278.85 | 4.73 | 10.0 | 8.6 |
| 52 | 927.26 | 278.40 | 4.86 | 27.0 | 25.3 |
| 53 | 929.89 | 278.71 | 4.77 | 12.5 | 12.0 |
| 54 | 925.03 | 278.13 | 4.94 | 41.0 | 47.0 |
| 55 | 920.08 | 277.55 | 5.12 | 206.0 | 178.3 |
| 56 | 951.60 | 277.01 | 5.29 | 946.0 | 570.8 |
| 57 | 932.29 | 278.99 | 4.69 | 6.0 | 6.0 |
| 58 | 928.11 | 278.50 | 4.83 | 14.0 | 19.9 |
| 59 | 925.57 | 278.20 | 4.92 | 30.0 | 40.5 |
| 60 | 924.19 | 278.03 | 4.97 | 39.0 | 59.1 |
| 61 | 930.80 | 278.82 | 4.74 | 12.0 | 9.3 |
| 62 | 929.32 | 278.64 | 4.79 | 18.0 | 14.1 |
| 63 | 925.84 | 278.23 | 4.91 | 35.0 | 37.6 |
| 64 | 922.77 | 277.87 | 5.02 | 98.0 | 86.9 |
| 65 | 921.16 | 277.67 | 5.08 | 141.0 | 133.9 |
| 66 | 921.16 | 277.67 | 5.08 | 150.0 | 133.9 |
| 67 | 914.58 | 276.89 | 5.33 | 846.0 | 739.7 |
| 68 | 913.30 | 276.74 | 5.38 | 1156.0 | 1021.2 |
| 69 | 926.73 | 278.34 | 4.88 | 37.0 | 29.3 |
| 70 | 927.30 | 278.40 | 4.86 | 23.0 | 25.0 |
| 71 | 923.59 | 277.96 | 4.99 | 66.0 | 69.6 |
| 72 | 919.77 | 277.51 | 5.13 | 196.0 | 193.5 |
| 73 | 921.16 | 277.67 | 5.08 | 156.0 | 133.9 |
| 74 | 914.83 | 276.92 | 5.32 | 971.0 | 694.3 |
| 75 | 913.30 | 276.74 | 5.38 | 1466.0 | 1021.2 |
| 76 | 917.95 | 277.29 | 5.20 | 396.0 | 311.6 |
| 77 | 947.31 | 280.76 | 4.22 | 0.0 | 0.1 |
| 78 | 945.97 | 280.60 | 4.26 | 0.0 | 0.1 |
| 79 | 940.69 | 279.98 | 4.42 | 0.0 | 0.5 |
| 80 | 938.11 | 279.68 | 4.50 | 0.0 | 1.1 |
| 81 | 937.51 | 279.61 | 4.52 | 3.5 | 1.3 |
| 82 | 934.06 | 279.20 | 4.63 | 4.0 | 3.6 |
| 83 | 934.06 | 279.20 | 4.63 | 5.0 | 3.6 |

observation is $N$ the number density of drops nucleated during the expansion. In order to account for the effects of an impurity causing heterogeneous nucleation, $N$ was decreased by 4 drops $cm^{-3}$ from the actual drop density observed. The existence of this level of background heterogeneous nucleation was indicated in studies employing an increased sensitive time nucleation pulse.[14] Drop concentrations less than 4 $cm^{-3}$ appear as 0.0 in the Tables. The run # is provided for identification of data points and does not denote the order in which measurements were made. Also included are $S_{peak}$ and $T_{min}$, the peak supersaturation ratio and minimum temperature corresponding to the pressure minimum.

TABLE III. See caption for Table I. Initial temperature $T_1$ = 24.5 °C. $P$ coefficient $C_{p1}$ = 67.0352, $C_{p2}$ = 255 949.0. $S$ coefficient $C_{s1}$ = 5.239 73, $C_{s2}$ = 28.5718, $C_{s3}$ = 73.7517, $C_{s4}$ = 120.075. $T$ coefficient $C_{t1}$ = 269.049, $C_{t2}$ = −82.8395, $C_{t3}$ = 44.7583, $C_{t4}$ = −27.3827.

| Run | $P_{min}$ | $T_{min}$ | $S_{peak}$ | $N$ | $\int J\,dt$ |
|---|---|---|---|---|---|
| 84 | 918.07 | 267.65 | 5.75 | 68.5 | 78.5 |
| 85 | 910.68 | 266.79 | 6.09 | 596.0 | 591.3 |
| 86 | 909.64 | 266.67 | 6.14 | 624.0 | 777.4 |
| 87 | 924.09 | 268.34 | 5.49 | 15.0 | 13.7 |
| 88 | 918.98 | 267.75 | 5.71 | 73.0 | 60.6 |
| 89 | 911.10 | 266.84 | 6.07 | 646.0 | 529.1 |
| 90 | 907.75 | 266.45 | 6.23 | 1316.0 | 1269.6 |
| 91 | 927.72 | 268.76 | 5.34 | 6.0 | 4.5 |
| 92 | 926.99 | 268.68 | 5.37 | 6.0 | 5.7 |
| 93 | 920.58 | 267.94 | 5.64 | 41.0 | 38.3 |
| 94 | 916.73 | 267.49 | 5.81 | 125.0 | 114.4 |
| 95 | 920.35 | 267.91 | 5.65 | 42.0 | 40.9 |
| 96 | 913.88 | 267.16 | 5.94 | 250.0 | 250.8 |
| 97 | 912.15 | 266.96 | 6.02 | 376.0 | 400.0 |
| 98 | 905.77 | 266.22 | 6.33 | 1396.0 | 2104.0 |
| 99 | 916.07 | 267.41 | 5.84 | 133.0 | 137.4 |
| 100 | 915.62 | 267.36 | 5.86 | 154.0 | 155.6 |
| 101 | 908.20 | 266.50 | 6.21 | 896.0 | 1130.5 |
| 102 | 924.33 | 268.37 | 5.48 | 7.0 | 12.7 |
| 103 | 926.25 | 268.59 | 5.40 | 9.0 | 7.1 |
| 104 | 926.99 | 268.68 | 5.37 | 10.0 | 5.7 |
| 105 | 922.91 | 268.21 | 5.54 | 18.0 | 19.4 |
| 106 | 922.68 | 268.18 | 5.55 | 28.0 | 20.7 |
| 107 | 920.33 | 267.91 | 5.65 | 36.0 | 41.2 |
| 108 | 919.89 | 267.86 | 5.67 | 66.0 | 46.7 |
| 109 | 915.85 | 267.39 | 5.85 | 136.0 | 146.0 |
| 110 | 916.51 | 267.47 | 5.82 | 194.0 | 121.6 |
| 111 | 913.64 | 267.13 | 5.95 | 196.0 | 267.7 |
| 112 | 913.23 | 267.08 | 5.97 | 236.0 | 299.1 |
| 113 | 913.02 | 267.06 | 5.98 | 316.0 | 316.6 |
| 114 | 912.59 | 267.01 | 6.00 | 396.0 | 355.4 |
| 115 | 910.03 | 266.71 | 6.12 | 496.0 | 701.8 |
| 116 | 911.10 | 266.84 | 6.07 | 696.0 | 529.1 |
| 117 | 909.63 | 266.67 | 6.14 | 746.0 | 779.4 |
| 118 | 907.57 | 266.43 | 6.24 | 1496.0 | 1329.8 |
| 119 | 905.96 | 266.24 | 6.32 | 1996.0 | 2005.2 |
| 120 | 943.07 | 270.52 | 4.76 | 0.0 | 0.0 |
| 121 | 942.22 | 270.42 | 4.79 | 0.0 | 0.0 |
| 122 | 940.54 | 270.23 | 4.85 | 0.0 | 0.1 |
| 123 | 939.16 | 270.07 | 4.90 | 0.0 | 0.1 |
| 124 | 938.35 | 269.98 | 4.93 | 0.0 | 0.1 |
| 125 | 936.18 | 269.73 | 5.01 | 0.0 | 0.3 |
| 126 | 936.18 | 269.73 | 5.01 | 0.0 | 0.3 |
| 127 | 935.39 | 269.64 | 5.04 | 0.0 | 0.4 |
| 128 | 931.24 | 269.16 | 5.20 | 0.0 | 1.5 |
| 129 | 929.71 | 268.99 | 5.26 | 1.4 | 5.4 |

TABLE IV. See caption for Table I. Initial temperature $T_1$ = 13.2 °C. $P$ coefficient $C_{p1}$ = 391.4609, $C_{p2}$ = 164 583.0. $S$ coefficient $C_{s1}$ = 5.811 06. $C_{s2}$ = 33.6382, $C_{s3}$ = 92.5424, $C_{s4}$ = = 161.083. $T$ coefficient $C_{t1}$ = 258.729, $C_{t2}$ = −79.9571, $C_{t3}$ = 43.3214, $C_{t4}$ = −26.7027.

| Run # | $P_{min}$ | $T_{min}$ | $S_{peak}$ | $N$ | $\int J\,dt$ |
|---|---|---|---|---|---|
| 130 | 916.25 | 257.17 | 6.51 | 11.3 | 11.4 |
| 131 | 911.87 | 256.68 | 6.75 | 47.0 | 40.6 |
| 132 | 910.27 | 256.50 | 6.84 | 73.0 | 63.7 |
| 133 | 907.16 | 256.15 | 7.02 | 191.0 | 149.9 |
| 134 | 898.36 | 255.16 | 7.56 | 1496.0 | 1468.5 |
| 135 | 916.25 | 257.17 | 6.51 | 9.6 | 11.4 |
| 136 | 914.21 | 256.94 | 6.62 | 23.3 | 20.8 |
| 137 | 908.71 | 256.33 | 6.93 | 112.0 | 98.2 |
| 138 | 906.29 | 256.05 | 7.07 | 238.0 | 189.5 |
| 139 | 917.01 | 257.26 | 6.47 | 14.0 | 9.1 |
| 140 | 905.97 | 256.02 | 7.09 | 187.0 | 206.5 |
| 141 | 900.89 | 255.44 | 7.40 | 871.0 | 777.4 |
| 152 | 915.88 | 257.13 | 6.53 | 8.5 | 12.7 |
| 142 | 912.59 | 256.76 | 6.71 | 31.0 | 33.1 |
| 144 | 909.05 | 256.36 | 6.91 | 76.0 | 89.4 |
| 145 | 916.63 | 257.21 | 6.49 | 8.0 | 10.2 |
| 146 | 895.27 | 254.81 | 7.76 | 1996.0 | 3126.7 |
| 147 | 917.56 | 257.32 | 6.44 | 6.5 | 7.7 |
| 148 | 902.99 | 255.68 | 7.27 | 481.0 | 453.0 |
| 149 | 903.81 | 255.77 | 7.22 | 521.0 | 365.8 |
| 150 | 898.20 | 255.14 | 7.57 | 1196.0 | 1528.0 |
| 151 | 924.60 | 258.10 | 6.08 | 0.0 | 0.9 |
| 152 | 925.44 | 258.20 | 6.04 | 0.0 | 0.7 |
| 153 | 927.49 | 258.42 | 5.94 | 0.0 | 0.3 |
| 154 | 922.42 | 257.86 | 6.19 | 0.0 | 1.7 |
| 155 | 924.01 | 258.04 | 6.11 | 0.0 | 1.0 |
| 156 | 924.62 | 258.11 | 6.08 | 0.0 | 0.9 |
| 157 | 919.68 | 257.55 | 6.33 | 1.9 | 4.9 |
| 158 | 919.10 | 257.49 | 6.36 | 4.0 | 4.8 |

TABLE V. See caption for Table I. Initial temperature $T_1$ = 3 °C. $P$ coefficient $C_{p1}$ = 67.0352, $C_{p2}$ = 255 949.0. $S$ coefficient $C_{s1}$ = 6.409 73, $C_{s2}$ = 39.1476, $C_{s3}$ = 114.071, $C_{s4}$ = 210.686. $T$ coefficient $C_{t1}$ = 249.457, $C_{t2}$ = −77.245, $C_{t3}$ = 41.9153, $C_{t4}$ = −25.7397.

| Run # | $P_{min}$ | $T_{min}$ | $S_{peak}$ | $N$ | $\int J\,dt$ |
|---|---|---|---|---|---|
| 159 | 905.78 | 246.82 | 7.92 | 4.5 | 14.3 |
| 160 | 899.83 | 246.17 | 8.35 | 68.0 | 69.9 |
| 161 | 895.63 | 245.71 | 8.67 | 51.0 | 201.9 |
| 162 | 899.97 | 246.18 | 8.34 | 31.0 | 67.4 |
| 163 | 904.65 | 246.69 | 8.00 | 20.0 | 19.5 |
| 164 | 901.18 | 246.32 | 8.25 | 57.0 | 49.2 |
| 165 | 897.06 | 245.86 | 8.56 | 121.0 | 141.4 |
| 166 | 893.98 | 245.53 | 8.80 | 338.0 | 302.4 |
| 167 | 892.22 | 245.33 | 8.94 | 524.0 | 461.8 |
| 168 | 888.11 | 244.88 | 9.28 | 1436.0 | 1205.0 |
| 169 | 899.83 | 246.17 | 8.35 | 63.0 | 69.9 |
| 170 | 889.30 | 245.01 | 9.18 | 1196.0 | 916.8 |
| 171 | 894.23 | 245.55 | 8.78 | 326.0 | 284.5 |
| 172 | 890.76 | 245.17 | 9.06 | 932.0 | 652.4 |
| 173 | 892.71 | 245.39 | 8.90 | 566.0 | 410.8 |
| 174 | 891.24 | 245.23 | 9.02 | 626.0 | 582.6 |
| 175 | 891.86 | 245.29 | 8.97 | 460.0 | 503.1 |
| 176 | 915.85 | 247.91 | 7.25 | 0.0 | 0.8 |
| 177 | 920.26 | 248.39 | 6.98 | 0.0 | 0.2 |
| 178 | 910.77 | 247.36 | 7.58 | 0.0 | 3.5 |
| 179 | 911.82 | 247.47 | 7.51 | 0.0 | 2.6 |
| 180 | 909.13 | 247.18 | 7.69 | 2.0 | 5.6 |
| 181 | 908.98 | 247.16 | 7.70 | 4.0 | 5.9 |

TABLE VI. See caption for Table I. Initial temperature $T_i = -3$ °C. $= -3$ °C. $P$ coefficient $C_{p1} = 459.5039$, $C_{p2} = 44\,927.0$. $S$ coefficient $C_{s1} = 6.262\,05$, $C_{s2} = 39.4815$, $C_{s3} = 119.053$, $C_{s4} = 227.969$. $T$ coefficient $C_{t1} = 244.015$, $C_{t2} = -75.6191$, $C_{t3} = 41.0677$, $C_{t4} = -25.2304$.

| Run | $P_{min}$ | $T_{min}$ | $S_{peak}$ | $N$ | $\int J\,dt$ |
|---|---|---|---|---|---|
| 182 | 888.17 | 239.54 | 9.17 | 10.0 | 14.5 |
| 183 | 882.65 | 238.95 | 9.66 | 69.0 | 59.4 |
| 184 | 880.28 | 238.69 | 9.88 | 103.0 | 106.1 |
| 185 | 877.44 | 238.38 | 10.15 | 198.0 | 208.6 |
| 186 | 875.48 | 238.17 | 10.34 | 349.0 | 328.5 |
| 187 | 874.79 | 238.09 | 10.41 | 307.0 | 384.5 |
| 188 | 889.69 | 239.71 | 9.04 | 7.0 | 9.7 |
| 189 | 885.99 | 239.31 | 9.36 | 28.0 | 25.6 |
| 190 | 883.84 | 239.08 | 9.55 | 43.0 | 44.1 |
| 191 | 882.31 | 238.91 | 9.69 | 68.0 | 64.6 |
| 192 | 879.85 | 238.64 | 9.92 | 121.0 | 117.7 |
| 193 | 875.90 | 238.21 | 10.30 | 372.0 | 298.2 |
| 194 | 888.52 | 239.58 | 9.14 | 15.0 | 13.2 |
| 195 | 884.53 | 239.15 | 9.49 | 40.0 | 37.1 |
| 196 | 882.64 | 238.95 | 9.66 | 69.0 | 59.6 |
| 197 | 877.96 | 238.44 | 10.10 | 191.0 | 184.6 |
| 198 | 875.70 | 238.19 | 10.32 | 341.0 | 321.3 |
| 199 | 875.30 | 238.15 | 10.36 | 251.0 | 342.3 |
| 200 | 890.64 | 239.81 | 8.96 | 7.5 | 7.5 |
| 201 | 887.37 | 239.46 | 9.24 | 18.0 | 17.9 |
| 202 | 882.76 | 238.96 | 9.65 | 78.0 | 57.8 |
| 203 | 882.54 | 238.93 | 9.67 | 56.0 | 61.0 |
| 204 | 880.91 | 238.76 | 9.82 | 110.0 | 91.1 |
| 205 | 875.90 | 238.21 | 10.30 | 351.0 | 298.2 |
| 206 | 871.25 | 237.71 | 10.77 | 1071.0 | 847.4 |
| 207 | 889.57 | 239.69 | 9.05 | 10.0 | 10.0 |
| 208 | 885.88 | 239.30 | 9.37 | 26.0 | 26.3 |
| 209 | 881.35 | 238.81 | 9.78 | 90.0 | 81.8 |
| 210 | 875.40 | 238.16 | 10.35 | 376.0 | 334.5 |
| 211 | 880.17 | 238.68 | 9.89 | 116.0 | 109.0 |
| 212 | 875.20 | 238.14 | 10.37 | 277.0 | 350.2 |
| 213 | 872.51 | 237.84 | 10.64 | 756.0 | 641.9 |
| 214 | 888.75 | 239.61 | 9.12 | 14.0 | 12.4 |
| 215 | 882.21 | 238.90 | 9.70 | 70.0 | 66.2 |
| 216 | 884.75 | 239.17 | 9.47 | 39.0 | 35.1 |
| 217 | 880.60 | 238.72 | 9.85 | 83.0 | 98.2 |
| 218 | 878.78 | 238.53 | 10.02 | 161.0 | 152.0 |
| 219 | 875.40 | 238.16 | 10.35 | 346.0 | 334.5 |
| 220 | 868.87 | 237.45 | 11.02 | 1496.0 | 1417.2 |
| 221 | 902.21 | 241.05 | 8.05 | 0.0 | 0.3 |
| 222 | 900.18 | 240.83 | 8.20 | 0.0 | 0.5 |
| 223 | 904.95 | 241.34 | 7.85 | 0.0 | 0.1 |
| 224 | 903.28 | 241.16 | 7.97 | 0.0 | 0.2 |
| 225 | 904.12 | 241.25 | 7.91 | 0.0 | 0.1 |
| 226 | 900.80 | 240.91 | 8.15 | 0.0 | 0.4 |
| 227 | 900.60 | 240.88 | 8.17 | 0.0 | 0.4 |
| 228 | 897.33 | 240.53 | 8.42 | 0.0 | 1.1 |
| 229 | 897.33 | 240.53 | 8.42 | 0.0 | 1.1 |
| 230 | 896.56 | 240.44 | 8.48 | 0.0 | 1.4 |
| 231 | 897.97 | 240.60 | 8.37 | 0.0 | 0.9 |
| 232 | 897.07 | 240.50 | 8.44 | 0.7 | 1.2 |
| 233 | 896.82 | 240.47 | 8.46 | 1.0 | 1.3 |
| 234 | 895.80 | 240.36 | 8.54 | 2.0 | 1.8 |
| 235 | 892.82 | 240.04 | 8.78 | 3.0 | 4.1 |
| 236 | 894.17 | 240.19 | 8.67 | 5.0 | 2.8 |
| 237 | 893.56 | 240.12 | 8.72 | 5.7 | 3.4 |

The next step was to derive an empirical nucleation rate formula by fitting $J$ in Eq. (1) to this data by minimizing $Y$ in Eq. (4). $Y$ is minimized by adjusting the $x$'s in Eqs. (2) and (3). The result is

$$J = S^2 \exp[328.124 - 5.582\,43T + 0.030\,365T^2 - 5.0319E - 5T^3 - (999.814 - 4.100\,87T + 3.010\,84E - 3T^2)/(\ln S)^2] . \quad (8)$$

The units of $J$ are drops $cm^{-3}\,s^{-1}$ and $T$ are K. This expression describes the nucleation rate of water from $J = 1$–$10^6$ drops $cm^{-3}\,s^{-1}$ over temperatures ranging from 230 to 290 K.

The quality of the fit of Eq. (8) to the experimental data can be seen in Fig. 3. The circles represent the experimentally observed drop densities, i.e., the $N$'s from Tables I–VII. The solid lines represent the corresponding drop densities as predicted by Eq. (8), i.e., $\int J\,dt$ from Tables I–VII for each experimental $S(t)$ and $T(t)$ profile. Both the 24.5 and 3 °C data sets include measurements taken weeks apart. The scatter of these points gives a clear indication of the repeatability of the experiment.

TABLE VII. See caption for Table I. Initial temperature $T_i = -9$ °C. $P$ coefficient $C_{p1} = 322.8750$, $C_{p2} = 25\,130.0$. $S$ coefficient $C_{s1} = 6.666\,09$, $C_{s2} = 43.3947$, $C_{s3} = 135.466$, $C_{s4} = 269.077$. $T$ coefficient $C_{t1} = 238.585$, $C_{t2} = -73.965$, $C_{t3} = 40.1876$, $C_{t4} = -24.7192$.

| Run# | $P_{min}$ | $T_{min}$ | $S_{peak}$ | $N$ | $\int J\,dt$ |
|---|---|---|---|---|---|
| 238 | 879.64 | 233.31 | 10.74 | 17.0 | 26.9 |
| 239 | 885.13 | 233.89 | 10.18 | 7.0 | 6.9 |
| 240 | 877.77 | 233.11 | 10.94 | 46.0 | 41.9 |
| 241 | 877.03 | 233.03 | 11.02 | 55.0 | 49.9 |
| 242 | 875.29 | 232.85 | 11.21 | 73.0 | 74.6 |
| 243 | 873.50 | 232.66 | 11.41 | 131.0 | 112.0 |
| 244 | 873.24 | 232.63 | 11.44 | 136.0 | 118.7 |
| 245 | 864.66 | 231.71 | 12.46 | 752.0 | 741.4 |
| 246 | 863.70 | 231.61 | 12.58 | 916.0 | 900.4 |
| 247 | 863.94 | 231.63 | 12.55 | 924.0 | 857.9 |
| 248 | 875.12 | 232.83 | 11.23 | 66.0 | 77.6 |
| 249 | 862.36 | 231.46 | 12.75 | 1496.0 | 1176.8 |
| 250 | 870.03 | 232.29 | 11.81 | 224.0 | 240.5 |
| 251 | 867.76 | 232.04 | 12.08 | 376.0 | 390.3 |
| 252 | 864.90 | 231.74 | 12.43 | 776.0 | 706.0 |
| 253 | 862.05 | 231.43 | 12.79 | 1216.0 | 1251.2 |
| 254 | 883.61 | 233.73 | 10.33 | 10.0 | 10.1 |
| 255 | 874.49 | 232.76 | 11.30 | 82.0 | 89.5 |
| 256 | 871.84 | 232.48 | 11.60 | 155.0 | 162.0 |
| 257 | 875.84 | 232.90 | 11.15 | 66.0 | 65.7 |
| 258 | 872.19 | 232.52 | 11.56 | 130.0 | 149.9 |
| 259 | 876.76 | 233.00 | 11.05 | 56.0 | 53.1 |
| 260 | 871.32 | 232.42 | 11.66 | 211.0 | 181.6 |
| 261 | 881.77 | 233.53 | 10.52 | 16.0 | 16.0 |
| 262 | 878.24 | 233.16 | 10.89 | 26.0 | 37.5 |
| 263 | 874.40 | 232.75 | 11.31 | 114.0 | 91.4 |
| 264 | 874.76 | 232.79 | 11.27 | 87.0 | 84.2 |
| 265 | 865.38 | 231.79 | 12.37 | 716.0 | 640.0 |
| 266 | 816.89 | 231.41 | 12.81 | 1724.0 | 1291.4 |
| 267 | 876.48 | 232.97 | 11.08 | 57.0 | 56.7 |
| 268 | 870.37 | 232.32 | 11.77 | 306.0 | 223.4 |
| 269 | 867.43 | 232.01 | 12.12 | 405.0 | 418.3 |
| 270 | 864.58 | 231.70 | 12.47 | 740.0 | 753.6 |
| 271 | 889.16 | 234.32 | 9.79 | 3.0 | 2.4 |
| 272 | 897.56 | 235.20 | 9.03 | 0.0 | 0.2 |
| 273 | 892.60 | 234.68 | 9.47 | 0.0 | 0.9 |
| 274 | 886.15 | 234.00 | 10.08 | 4.0 | 5.3 |
| 275 | 887.89 | 234.18 | 9.91 | 4.5 | 3.4 |

Since our expansion chamber's features allow us to extract the nucleation rate directly, our nucleation rate data is not necessarily directly comparable with ordinary critical supersaturation measurements. We can, however, extract from our results a critical supersaturation defined by $J = 1\ \mathrm{cm^{-3}\,s^{-1}}$ as a function of temperature and compare these results with other works. This is shown in Fig. 4. The agreement between our results and those of Heist and Reiss[19] (static thermal diffusion chamber results) is quite good, both in the position of the data and in the general shape of the curves. The data of Volmer and Flood[20] and Sharrer[21] is relatively old and contains much larger uncertainties in temperature, supersaturation, and nucleation rate. Allard and Kassner[8] showed how both the natural sensitive time of the cloud chamber and the type of observation system employed must be taken into account in the intercomparison of data from some of the older literature.

Wagner and Strey recently measured homogeneous nucleation rates[22] for water in the very high rate regime $2\times10^{5}$–$2\times10^{9}\ \mathrm{cm^{-3}\,s^{-1}}$. Their measurements and ours cover different ranges of nucleation rates, but show some overlap at nucleation rates around $2\times10^{5}\ \mathrm{cm^{-3}\,s^{-1}}$, where they agree within a factor of ~2.

It is important to verify that the observed nucleation is indeed homogeneous and not compromised by heterogeneous impurities. We have found three checks which are useful for identifying whether or not the observed nucleation is homogeneous. First, the nucleation rate should not decay with time. This can be examined by employing variable sensitive time nucleation pulses. Second, the critical supersaturation ratio (for a given nucleation rate, e.g., $1\ \mathrm{cm^{-3}\,s^{-1}}$) should smoothly increase as the temperature decreases (such as the behavior shown in Fig. 4). This is the least sensitive technique for detecting heterogeneous impurities because it requires that the impurity exhibit a strong temperature dependence either in its activity or the reaction rate constants involved in the reactions which form the impurity. Third, a plot of the logarithm of drop concentration vs supersaturation ratio for various temperatures (such as that shown in Fig. 3) should exhibit smooth behavior. The presence of a discontinuity or "knee" in a curve is indicative of a heterogeneous nucleant which is in small enough concentration to suffer noticeable depletion as a consequence of nucleating a number density of droplets comparable to that being observed during the experiment. Moreover, the separation of curves for data taken at different temperatures should follow an orderly progression not too different from the general predictions of the classical theory. While we feel that the above mentioned criteria are essential features of homogeneous nucleation, they are not necessarily a sufficient condition since the number of heterogeneous or bimolecular nucleation processes possible must form almost an infinite array, the distinguishing characteristic being the increment by which the free energy of formation is altered. However, the data from our chamber does exhibit all the essential characteristics of homogeneous nucleation that we have set forth above.[14]

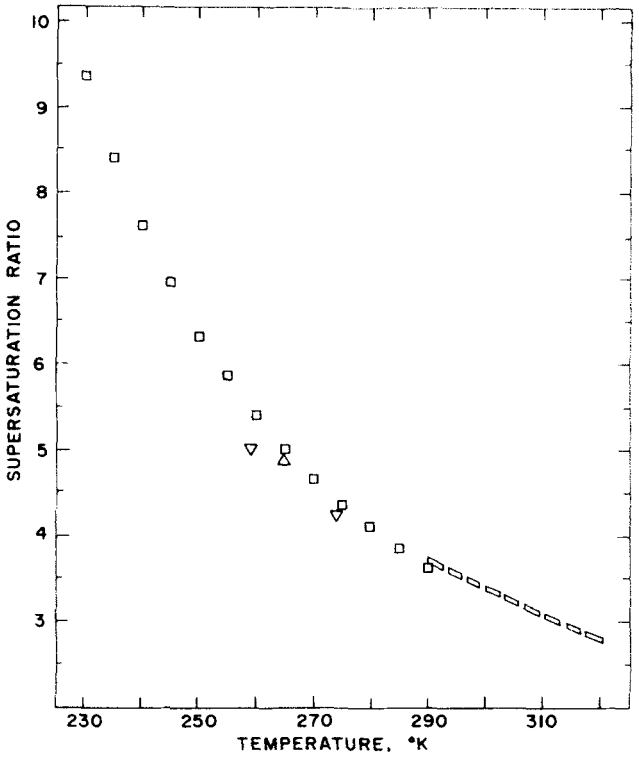


FIG. 4. Experimental measurements of the supersaturation and temperature for the onset of nucleation, $J = 1\ \mathrm{cm^{-3}\,s^{-1}}$. □: this work, □: Heist and Reiss (Ref. 19), ▽: Volmer and Flood (Ref. 20), △: Scharrer (Ref. 21).

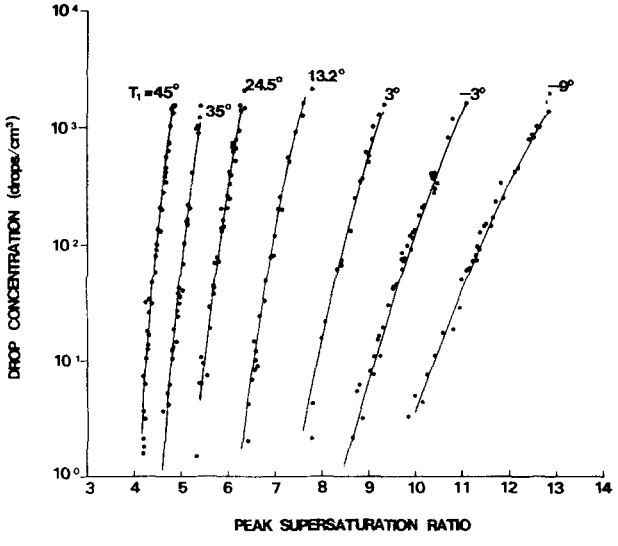


FIG. 3. Drop concentration vs supersaturation ratio. The circles represent the experimentally observed drop densities. The solid lines represent the drop densities corresponding to our empirical nucleation rate formula Eq. (8).

## IV. CONCLUSION

The nucleation measurements for water reported here represent a significant improvement over previously available data. The empirical nucleation rate Eq. (8) provides a quantitative description as well as allowing any investigator to make a detailed comparison with

theory. It covers a wide range of temperature, 230 – 290 K, and nucelation rate, $1–10^6$ drops $cm^{-3}$ $s^{-1}$. The ability to obtain this set of data was made possible by several advantageous features of the expansion cloud chamber: the fast pulse technique which separates nucleation and growth phenomena and which allows high nucleation rates to be sampled for very short times (yielding manageable drop counts), the use of cleaning expansions to remove interfering heterogeneous impurities, and its access to a wide range of operating temperatures.

## ACKNOWLEDGMENT

This material is based on work supported by the Division of Atmospheric Sciences, National Science Foundation under Grant ATM79-19480.

[1]S. Coulier, F. Pharm. Chim. Paris **22**, 165 (1875).
[2]J. Kiessling, Nachr. koniglich Ges. Wiss., Göttingen, **8**, 226 (1884).
[3]J. Aitken, Nature (London) **23**, 195 (1880).
[4]C. T. R. Wilson, Philos. Trans. R. Soc. A **189**, 265 (1897).
[5]C. T. R. Wilson, Proc. R. Soc. (London) **85**, 285 (1911).
[6]B. J. Mason, *Physics of Clouds*, 1st ed. (Oxford University, London, 1957).
[7]R. J. Anderson, R. C. Miller, J. L. Kassner, Jr., and D. E. Hagen, J. Atmos. Sci. **37**, 2508 (1980).
[8]E. F. Allard and J. L. Kassner, Jr., J. Chem. Phys. **42**, 1401 (1965).
[9]J. L. Kassner, Jr. and R. L. Schmitt, J. Chem. Phys. **44**, 4166 (1966).
[10]J. L. Kassner, Jr., J. C. Carstens, and L. B. Allen, J. Atmos. Sci. **25**, 919 (1968).
[11]L. B. Allen and J. L. Kassner, Jr., J. Colloid Int. Sci. **30**, 81 (1969).
[12]J. L. Schmitt, Rev. Sci. Instrum. **52**, 109 (1981).
[13]D. E. Hagen, R. J. Anderson, and J. L. Kassner, Jr., J. Atmos. Sci. **38**, 1236 (1981).
[14]D. E. Hagen, J. L. Kassner, Jr., and R. C. Miller, J. Atmos. Sci. (to be published).
[15]*Handbook of Chemistry and Physics*, 50th ed., edited by R. C. Weast (Chemical Rubber Co., Cleveland, 1969).
[16]R. D. H. Low, J. Atmos. Sci. **26**, 608 (1969).
[17]B. N. Hale and P. L. M. Plummer, J. Chem. Phys. **61**, 4012 (1974).
[18]J. P. Chandler, Quantum Chemistry Program Exchange, Indiana University, 1965.
[19]R. Heist and H. Reiss, J. Chem. Phys. **59**, 665 (1973).
[20]M. Volmer and H. Z. Flood, Z. Phys. Chem. A **190**, 273 (1934).
[21]I. Scharrer, Ann. Phys. **35**, 619 (1939).
[22]P. E. Wagner and R. Strey, J. Phys. Chem. **85**, 2694 (1981).